ACS ES&T Water

pubs.acs.org/estwater

Article



# Modeling pH-Dependent Adsorption of Glyphosate on Iron Hydroxides: Competition with Phosphate and Influence of $Fe^{2+}$

Mingshuai Wang, Johannes Lützenkirchen, and Stefan B. Haderlein*

Cite This: *ACS EST Water* 2026, 6, 2018−2028

Read Online

ACCESS | Metrics & More | Article Recommendations | Supporting Information

**ABSTRACT:** Understanding and predicting the glyphosate (Gly) migration at the water−soil interface remains a critical challenge in environmental pollution control. Iron hydroxides, particularly goethite and ferrihydrite, serve as important sinks for pollutants and are significant for geochemical modeling. This study systematically investigates the pH-dependent competitive adsorption of Gly and phosphate ($PO_4$) on these iron minerals, alongside the influence of ferrous ions ($Fe^{2+}$) on Gly adsorption—a process whose mechanistic background remains inadequately explored in previous studies. Utilizing the Charge Distribution Multisite Surface Complexation (CD-MUSIC) model, we analyzed adsorption data to evaluate surface complexation constants (log K), binding mechanisms, and competitive effects. Results revealed that Gly and $PO_4$ adsorption is primarily governed by pH, concentration, mineral type, and competitive interactions, with $PO_4$ significantly suppressing Gly retention. Nevertheless, Gly maintains measurable adsorption even under strong competition, attributed to irreversible bidentate complexation. The model's underestimation at higher loadings further points to the likely role of steric hindrance effects, a factor not accounted for in the current CD-MUSIC formulation. $Fe^{2+}$ exhibits dual roles: it enhances Gly adsorption on ferrihydrite via coadsorption, potentially via electrostatic attraction and possible on distinct sorption sites, while its impact on goethite is negligible. These findings underscore the $PO_4$ critical role in reducing Gly retention in iron-rich soils and highlight the context-dependent influence of $Fe^{2+}$. Our work advances the application of CD-MUSIC modeling to complex organic−inorganic systems and provides insights for optimizing soil remediation to mitigate Gly leaching.

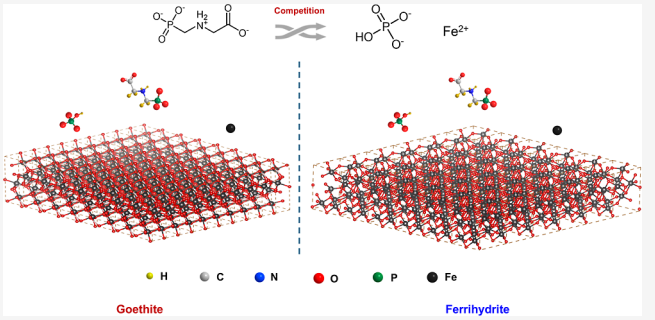


**KEYWORDS:** *glyphosate, phosphate, ferrous ions, goethite, ferrihydrite, CD-MUSIC*



## 1. INTRODUCTION

Glyphosate (*N*-(phosphonomethyl)glycine, Gly), the most widely used broad-spectrum herbicide globally, has an estimated average annual application rate in European countries of 0.62 kg per hectare from 2011 to 2017.[1] Its environmental persistence has been well-documented, with residues detected in soils, surface waters, and groundwater systems,[2−5] raising significant concerns about its environmental impact. These issues necessitate a comprehensive understanding of Gly behavior in natural systems, particularly its interactions with soil minerals and competing ions.

As a key nutrient supporting global agricultural productivity, phosphate ($PO_4$) shares structural and chemical similarities with Gly. This leads to competitive adsorption onto soil minerals—a process critical for environmental mobility and bioavailability of both compounds.[6,7] Iron hydroxides such as goethite and ferrihydrite, due to their high surface reactivity and widespread distribution in soils and sediments, serve as primary sorbents for these anions. Ferrous iron ($Fe^{2+}$), produced through anaerobic microbial respiration or mineral dissolution, further complicates the dynamics by catalyzing mineral recrystallization, altering surface charge through reductive dissolution,[8,9] and forming soluble complexes with Gly,[10] that may enhance its mobility. However, there is no consensus on Gly surface complexation structures on mineral surfaces and its binding modes under competitive adsorption, which is ultimately relevant for understanding and modeling its pH- and concentration-dependent environmental transport.

Previous studies have employed various characterization techniques and density functional theory (DFT) calculations[11−14] to analyze Gly surface speciation on minerals. Based on attenuated total reflection Fourier-transformed infrared (ATR-FTIR) spectroscopy interpretation, Barja and Afonso[12] proposed bridging bidentate adsorption configurations on goethite surfaces for pH 3.5−9.2 and at low-to-medium surface

Received: January 14, 2026
Revised: February 26, 2026
Accepted: February 26, 2026
Published: March 5, 2026

coverage. By contrast, Yan and Jing[13] demonstrated pH-dependent transitions from binuclear/mononuclear bidentate complexes under acidic conditions to mononuclear monodentate forms at higher pH using combined spectroscopic and DFT approaches. Another molecular dynamics simulation study[14] suggested the presence of intramolecular hydrogen bonding between the Gly phosphonate and amino groups and proposed adsorption primarily via monodentate complexation on goethite. The lack of a solid foundation for interpreting these spectroscopic and computational results has led to divergent conclusions across studies.

Similar research has analyzed the adsorption of $PO_4$ and $Fe^{2+}$ on goethite,[15−20] Kubicki et al.[15,16] discussed DFT-assisted modeling of $PO_4$ adsorption on goethite. By comparing simulations with experimental characterization, they concluded that $PO_4$ tends to form bidentate bridging surface complexes at low pH. For $Fe^{2+}$ adsorption on goethite, besides known mono- and bidentate complexes, studies have also indicated electron transfer from $Fe^{2+}$ to ferric iron ($Fe^{3+}$)[19] and the formation of tridentate complexes involving double edge-sharing.[20] Given its high stability and crystallinity, goethite has been the primary focus of most research, while studies on Gly complexation with other iron minerals, such as ferrihydrite, remain scarce.

Although these studies provide new insights into adsorption in single-solute systems, predictive modeling of binary adsorption remains challenging. Established surface complexation models (SCMs), such as the Charge Distribution Multisite Complexation (CD-MUSIC) model, quantify ligand binding affinities at the mineral/water interface. The CD-MUSIC model achieves this by dissecting electrostatic contributions through CD parameters, which are often derived from molecular orbital/density functional theory (MO/DFT) analysis.[21] These frameworks make SCMs particularly adept at identifying changes in surface complexation structures with pH and loading. Their predictive power has been successfully evidenced by the adsorption of metal ions[22−24] and oxyanions.[25−27] In contrast, the application of such models to organic molecules featuring multiple functional groups remains far less explored. In a recent key advance, Geysels and Hiemstra[28] established a set of CD-MUSIC parameters that comprehensively describes the pH- and loading-dependent sorption behavior of Gly on goethite, providing a foundation for extending this modeling approach to complex binary organic−inorganic adsorption systems.

Consequently, our work employs the CD-MUSIC framework to investigate the pH-dependent adsorption behavior of Gly on iron hydroxide, with particular emphasis on its competitive interactions with $PO_4$ and the influence of $Fe^{2+}$. By combining systematic adsorption experiments with CD values derived from prior studies, we optimize the corresponding affinity constants (log K) to interrogate surface complexation mechanisms in both $PO_4$-Gly and $Fe^{2+}$-Gly systems. In doing so, this study extends beyond previous work by explicitly testing CD-MUSIC predictions under higher surface loadings, stronger organic−inorganic competition, and mineralogical variability between crystalline goethite and poorly crystalline ferrihydrite. Importantly, the incorporation of $Fe^{2+}$ introduces an additional dimension that has rarely been addressed in SCM-based descriptions of Gly adsorption, despite its environmental relevance in redox-dynamic soils. Together, these advances enable a critical evaluation of the strengths and current limitations of equilibrium SCMs for describing organic−inorganic interactions at mineral−water interfaces. The resulting insights improve our mechanistic understanding of Gly fate in iron-rich soil and advance predictive capabilities for environmental risk management and remediation strategies.

## 2. MATERIALS AND METHODS

### 2.1. Chemicals and Materials

The chemicals used included glyphosate (96%, Sigma-Aldrich), potassium dihydrogen phosphate ($KH_2PO_4$, ≥99.5%, Merck), and iron(II) chloride tetrahydrate ($FeCl_2{\cdot}4H_2O$, 99.99%, Sigma-Aldrich), all of which were obtained as commercial reagents. HEPES buffer (≥99.5%, Sigma-Aldrich) was utilized to maintain a stable pH of 7. Potassium chloride (KCl, 99.0−100.5%, Sigma-Aldrich) was employed in some experiments as the background electrolyte for experiments conducted at other pH throughout the sorption studies. All chemicals used for synthesis and quantitative analysis were of analytical grade. Laboratory solutions were prepared with ultrapure water (0.057 $\mu$S/cm) (GenPure Pro UV, Thermo Fisher Scientific, Germany) and stored at a 4 °C fridge in the dark prior to use.

Goethite was synthesized following the method described by Schwertmann and Cornell,[29] resulting in a $N_2$−Brunauer−Emmett−Teller ($N_2$−BET) specific surface area (SSA) of 41.9 $m^2$/g. Synthetic two-line ferrihydrite[30] was prepared and used in all adsorption and titration experiments as a fresh suspension. A separate aliquot of the same batch was freeze−dried solely for characterization, yielding a BET SSA of 275.2 $m^2$/g. It should be noted that the $N_2$−BET−$SSA_{Feh}$ generally underestimates the real SSA due to irreversible aggregation of the particles during freeze-drying and outgassing.[31] Therefore, for all CD-MUSIC modeling in this study, the $SSA_{Feh}$ was set to 611 $m^2$/g,[32] representing the standard value for fresh ferrihydrite suspensions. Detailed synthesis and characterization are provided in Supporting Information (Figure S1 for BET analysis, Figure S2 for X-ray diffraction patterns).

### 2.2. Batch Sorption Experiments

All suspensions contained a background electrolyte of 0.02 M. Single and binary adsorption of Gly (0.05−2 mM) and $PO_4$ (0.05−2 mM) onto goethite (2.5 g/L) and ferrihydrite (0.17 g/L) was investigated through batch experiments at equilibrium pH 6, 7, and 8. These adsorption experiments were conducted under normal laboratory atmospheric conditions, as no $Fe^{2+}$ was involved. Furthermore, the influence of $CO_2$ on the adsorption system was considered negligible; its potential effects on mineral surface charge and system concentration are discussed in Figure S3. Stock solutions of Gly and $PO_4$, as well as iron mineral suspensions, were preadjusted to the target pH using HCl (0.1−1 M) and KOH (0.1−1 M) prior to mixing. The equivalent stock target solution was then added to the suspension to achieve the desired final concentrations. For binary competitive systems, Gly and $PO_4$ were always introduced simultaneously and at equal concentrations across the same range (0.05−2 mM) to simulate a cocontamination scenario with a fixed 1:1 molar ratio. $Fe^{2+}$ (0.05−2 mM) sorption experiments, conducted in the absence of $PO_4$ to isolate the binary $Fe^{2+}$-Gly interaction, were performed in an $N_2$-glovebox ($O_2$ < 0.1 ppm) (UNIlab plus, MBRAUN, Germany) to prevent $O_2$-driven redox reactions at pH 7. Notably, all solutions and suspensions were purged with helium (∼1 h) prior to transferring into the glovebox to eliminate the effects of dissolved $O_2$. Binary sorption involved pre-equilibration with Gly (0.24 mM) before the addition of $Fe^{2+}$. All samples were incubated in Falcon tubes and shaken for 12 h on a on a horizontal shaker (HS 501, IKA, Germany). Subsequently, the pH of each suspension was remeasured using a pH meter equipped with an ORP electrode (Seven2Go, Mettler Toledo, Switzerland), and phase separation was achieved by centrifugation at 12,000 rcf for 10 min to ensure complete sedimentation of colloidal particles for analysis.

The aqueous concentrations of Gly and $PO_4$ were quantified using ion chromatography (883 Basic IC plus, Metrohm, Switzerland) coupled with a conductivity detector (method description in Supporting Information, Figure S4) and by an ultraviolet−visible


https://doi.org/10.1021/acsestwater.6c00065
ACS EST Water 2026, 6, 2018−2028

**Table 1. Estimated Log K and CD Values for Gly, $PO_4$, and $Fe^{2+}$ Sorption on the Coordinated Surface Sites of Goethite[abcdef]**

| complexation equation | form | log K | $\Delta z_0$ | $\Delta z_1$ | $\Delta z_2$ |
|---|---|---|---|---|---|
| $\equiv FeOH^{-0.5} + H^+ \leftrightarrow \equiv FeOH_2^{+0.5}$ | | 9.25 | 1 | 0 | 0 |
| $\equiv Fe_3O^{-0.5} + H^+ \leftrightarrow \equiv Fe_3OH^{+0.5}$ | | 9.25 | 1 | 0 | 0 |
| $\equiv FeOH^{-0.5} + H^+ + Cl^- \leftrightarrow \equiv FeOH_2^{+0.5}\cdots Cl^-$ | | 8.95 | 1 | −1 | 0 |
| $\equiv FeOH^{-0.5} + K^+ \leftrightarrow \equiv FeOH^{-0.5}\cdots K^+$ | | −0.3 | 0 | 1 | 0 |
| $\equiv Fe_3O^{-0.5} + H^+ + Cl^- \leftrightarrow \equiv Fe_3OH^{+0.5}\cdots Cl^-$ | | 8.95 | 1 | −1 | 0 |
| $\equiv Fe_3O^{-0.5} + K^+ \leftrightarrow \equiv Fe_3O^{-0.5}\cdots K^+$ | | −0.3 | 0 | 1 | 0 |
| $2\equiv FeOH^{-0.5} + 2H^+ + Gly^{-3} \leftrightarrow \equiv Fe_2Gly^{-2} + 2H_2O$ | B | 21.15 | 0.69[28] | −0.95[28] | −0.74[28] |
| $\equiv FeOH^{-0.5} + 2H^+ + Gly^{-3} \leftrightarrow \equiv FeHGly^{-1.5} + H_2O$ | MH | 15.40 | 0.28[28] | −0.54[28] | −0.74[28] |
| $2\equiv FeOH^{-0.5} + 3H^+ + Gly^{-3} \leftrightarrow \equiv Fe_2HGly^{-1} + 2H_2O$ | BH | 29.75 | 0.75[28] | −0.01[28] | −0.74[28] |
| $\equiv FeOH^{-0.5} + 3H^+ + Gly^{-3} \leftrightarrow \equiv FeH_2Gly^{-0.5} + H_2O$ | $MH_2$ | 20.79 | 0.41[28] | 0.33[28] | −0.74[28] |
| $2\equiv FeOH^{-0.5} + 2H^+ + PO_4^{-3} \leftrightarrow \equiv Fe_2PO_4^{-2} + 2H_2O$ | B | 26.71 | 0.46[42] | −1.46[42] | 0[42] |
| $\equiv FeOH^{-0.5} + 2H^+ + PO_4^{-3} \leftrightarrow \equiv FeHPO_4^{-1.5} + H_2O$ | MH | 26.52 | 0.28[42] | −1.28[42] | 0[42] |
| $2\equiv FeOH^{-0.5} + 3H^+ + PO_4^{-3} \leftrightarrow \equiv Fe_2HPO_4^{-1} + 2H_2O$ | BH | 33.45 | 0.63[42] | −0.63[42] | 0[42] |
| $\equiv FeOH^{-0.5} + 3H^+ + PO_4^{-3} \leftrightarrow \equiv FeH_2PO_4^{-0.5} + H_2O$ | $MH_2$ | 33.25 | 0.33[38] | −0.33[38] | 0[38] |
| $\equiv FeOH^{-0.5} + Fe^{2+} \leftrightarrow \equiv FeOHFe_{II}^{+1.5}$ | M | 5.83 | 1.00 | 1.00 | 0 |
| $2\equiv FeOH^{-0.5} + Fe^{2+} \leftrightarrow \equiv (FeOH)_2Fe_{II}^{+1}$ | B | 9.35 | 0.73[19] | 1.27[19] | 0[19] |
| $2\equiv FeOH^{-0.5} + Fe^{2+} + 2H_2O \leftrightarrow \equiv (FeOH)_2Fe_{III}(OH)_2^{-1} + 2H^+$ | B + $e^-$ | −8.74 | 0.17[19] | −0.17[19] | 0[19] |
| $2\equiv FeOH^{-0.5} + \equiv Fe_3O^{-0.5} + Fe^{2+} \leftrightarrow \equiv (FeOH)_2(Fe_3O)\ Fe_{II}^{+0.5}$ | T | 6.99 | 1.26[19] | 0.74[19] | 0[19] |

[a]The CD factors are referenced from previous CD-MUSIC model studies. [b]ref 19 taken from Hiemstra, T. & van Riemsdijk, W. H., 2007.ref [c]ref 28 taken from Geysels, B. et al., 2025. [d]ref 38 taken from Hiemstra, T. & Zhao, W., 2016. [e]ref 42 taken from Rahnemaie, R. & Hiemstra, T., 2007. [f]M and B refer to monodentate and bidentate complexes, respectively.

**Table 2. Estimated Log K and CD Values for Gly, $PO_4$, and $Fe^{2+}$ Sorption on the Coordinated Surface Sites of Ferrihydrite[abcdef]**

| complexation equation | form | log K | $\Delta z_0$ | $\Delta z_1$ | $\Delta z_2$ |
|---|---|---|---|---|---|
| $\equiv FeO_cH^{-0.5} + H^+ \leftrightarrow \equiv FeO_cH_2^{+0.5}$ | | 8.01 | 1 | 0 | 0 |
| $\equiv FeO_cH^{-0.5} + H^+ \leftrightarrow \equiv FeO_cH_2^{+0.5}$ | | 8.01 | 1 | 0 | 0 |
| $\equiv Fe_3O^{-0.5} + H^+ \leftrightarrow \equiv Fe_3OH^{+0.5}$ | | 8.01 | 1 | 0 | 0 |
| $\equiv FeO_cH^{-0.5} + H^+ + Cl^- \leftrightarrow \equiv FeO_cH_2^{+0.5}\cdots Cl^-$ | | 7.74 | 1 | −1 | 0 |
| $\equiv FeO_cH^{-0.5} + K^+ \leftrightarrow \equiv FeO_cH^{-0.5}\cdots K^+$ | | −0.6 | 0 | 1 | 0 |
| $\equiv FeO_cH^{-0.5} + H^+ + Cl^- \leftrightarrow \equiv FeO_cH_2^{+0.5}\cdots Cl^-$ | | 7.74 | 1 | −1 | 0 |
| $\equiv FeO_cH^{-0.5} + K^+ \leftrightarrow \equiv FeO_cH^{-0.5}\cdots K^+$ | | −0.6 | 0 | 1 | 0 |
| $\equiv Fe_3O^{-0.5} + H^+ + Cl^- \leftrightarrow \equiv Fe_3OH^{+0.5}\cdots Cl^-$ | | 7.74 | 1 | −1 | 0 |
| $\equiv Fe_3O^{-0.5} + K^+ \leftrightarrow \equiv Fe_3O^{-0.5}\cdots K^+$ | | −0.6 | 0 | 1 | 0 |
| $2\equiv Fe_cOH^{-0.5} + 2H^+ + Gly^{-3} \leftrightarrow \equiv Fe_2Gly^{-2}(c) + 2H_2O$ | B | 22.15 | 0.69[28] | −0.95[28] | −0.74[28] |
| $\equiv FeOH^{-0.5} + 2H^+ + Gly^{-3} \leftrightarrow \equiv FeHGly^{-1.5} + H_2O$ | MH | 17.40 | 0.28[28] | −0.54[28] | −0.74[28] |
| $2\equiv Fe_cOH^{-0.5} + 3H^+ + Gly^{-3} \leftrightarrow \equiv Fe_2HGly^{-1}(c) + 2H_2O$ | BH | 26.82 | 0.75[28] | −0.01[28] | −0.74[28] |
| $\equiv FeOH^{-0.5} + 3H^+ + Gly^{-3} \leftrightarrow \equiv FeH_2Gly^{-0.5} + H_2O$ | $MH_2$ | 21.79 | 0.41[28] | 0.33[28] | −0.74[28] |
| $2\equiv Fe_cOH^{-0.5} + 2H^+ + PO_4^{-3} \leftrightarrow \equiv Fe_2PO_4^{-2}(c) + 2H_2O$ | B | 28.31 | 0.46[38,42] | −1.46[38,42] | 0[38,42] |
| $\equiv FeOH^{-0.5} + 2H^+ + PO_4^{-3} \leftrightarrow \equiv FeHPO_4^{-1.5} + H_2O$ | MH | 23.88 | 0.28[38,42] | −1.28[38,42] | 0[38,42] |
| $2\equiv Fe_cOH^{-0.5} + 3H^+ + PO_4^{-3} \leftrightarrow \equiv Fe_2HPO_4^{-1}(c) + 2H_2O$ | BH | 33.52 | 0.65[38] | −0.65[38] | 0[38] |
| $\equiv FeOH^{-0.5} + 3H^+ + PO_4^{-3} \leftrightarrow \equiv FeH_2PO_4^{-0.5} + H_2O$ | $MH_2$ | 30.22 | 0.33[38] | −0.33[38] | 0[38] |
| $\equiv FeOH^{-0.5} + Fe^{2+} \leftrightarrow \equiv FeOHFe_{II}^{+1.5}$ | M | 6.41 | 1.00 | 1.00 | 0 |
| $2\equiv Fe_cOH^{-0.5} + Fe^{2+} \leftrightarrow \equiv (FeOH)_2Fe_{II}^{+1}(c)$ | B | 10.13 | 0.73[19] | 1.27[19] | 0[19] |
| $2\equiv Fe_cOH^{-0.5} + Fe^{2+} + 2H_2O \leftrightarrow \equiv (FeOH)_2Fe_{III}(OH)_2^{-1}(c) + 2H^+$ | B + $e^-$ | −8.40 | 0.17[19] | −0.17[19] | 0[19] |
| $2\equiv Fe_cOH^{-0.5} + \equiv Fe_3O^{-0.5} + Fe^{2+} \leftrightarrow \equiv (FeOH)_2(Fe_3O)\ Fe_{II}^{+0.5}(c)$ | T | 5.41 | 1.26[19] | 0.74[19] | 0[19] |
| $\equiv Fe_3O^{-0.5} + Fe^{2+} \leftrightarrow \equiv Fe_3OFe_{II}^{+1.5}$ | M | 6.41 | 1.00 | 1.00 | 0 |

[a]The CD values are referenced from previous CD-MUSIC model studies. [b]ref 19 Taken from Hiemstra, T. & van Riemsdijk, W. H., 2007. [c]ref 28 Taken from Geysels, B. et al., 2025. [d]ref 38 Taken from Hiemstra, T. & Zhao, W., 2016. [e]ref 42 Taken from Rahnemaie, R. & Hiemstra, T., 2007. [f]M and B refer to monodentate and bidentate complexes, respectively.

spectrophotometer (UV5Bio, Mettler Toledo, Switzerland) via the molybdenum blue method,[33] respectively. Prior to $Fe^{2+}$ analysis, samples were acidified with 1 M HCl to stabilize $Fe^{2+}$.[34] The $Fe^{2+}$ concentration was then determined using the ferrozine assay.[35]

## 2.3. Titration and CD-MUSIC Modeling

The surface properties of goethite and ferrihydrite were characterized by acid−base titration using a titrator (836 Titrando, Metrohm, Switzerland). For each mineral, separate suspensions were prepared for titration at each background electrolyte concentration (0.01 and 0.1 M KCl). HCl (0.01 M) and KOH (0.01 M) solutions were used as titrants. For a given suspension, a complete forward (base) and backward (acid) titration cycle was performed on the same sample. Each titration began by acidifying the suspension to pH 4 with HCl, followed by a titration with KOH at a rate of 0.2 mL/min. At each step, the suspension was allowed to stabilize until the pH drift was less than 1 mV/min. To prevent $CO_2$ interference, the titration system was continuously purged with $N_2$. The total solid suspension surface area at the start of the titration was at least 10 $m^2$.[36] Raw data were processed based on theoretical blank titrations corrected for proton


https://doi.org/10.1021/acsestwater.6c00065
ACS EST Water 2026, 6, 2018−2028

**Table 3. Comparison of CD-MUSIC Parameters in This Study and Literature**[a,b]

| mineral | SSA ($m^2$/g) | $pH_{pzc}$ | $N_{s1}$ (site/$nm^2$) | $N_{s2}$ (site/$nm^2$) | $C_1$ (F/$m^2$) | $C_2$ (F/$m^2$) | ref |
|---|---|---|---|---|---|---|---|
| goethite | 94 | 9.3 | 3.45 | 2.7 | 0.83 | 0.74 | 28 |
| | 85 | / | / | / | 0.92 | 0.92 | 42 |
| | 23 | 9 | 4.78 | 2.08 | 1.86 | 3 | 43 |
| | 42 | 9.25 | 3.45 | 2.7 | 1.65 | 0.74 | this study |
| ferrihydrite | 615 | 8.1 | 5.8 | 1.4 | 1.15 | 0.9 | 38 |
| | 611 | / | 5.8 | 1.4 | / | / | 32 |
| | 229 | 8.7 | 6 | 1.2 | 0.74 | 0.93 | 44 |
| | 611 | 8.01 | 5.8 | 1.4 | 1.15 | 0.9 | this study |

[a]For ferrihydrite, $N_{s1}$ is the sum of site densities for two singly coordinated groups (≡$FeO_eH$ + ≡$FeO_cH$). [b]$N_{s1}$ and $N_{s2}$ indicate the site densities for singly and triply coordinated surface groups, respectively.

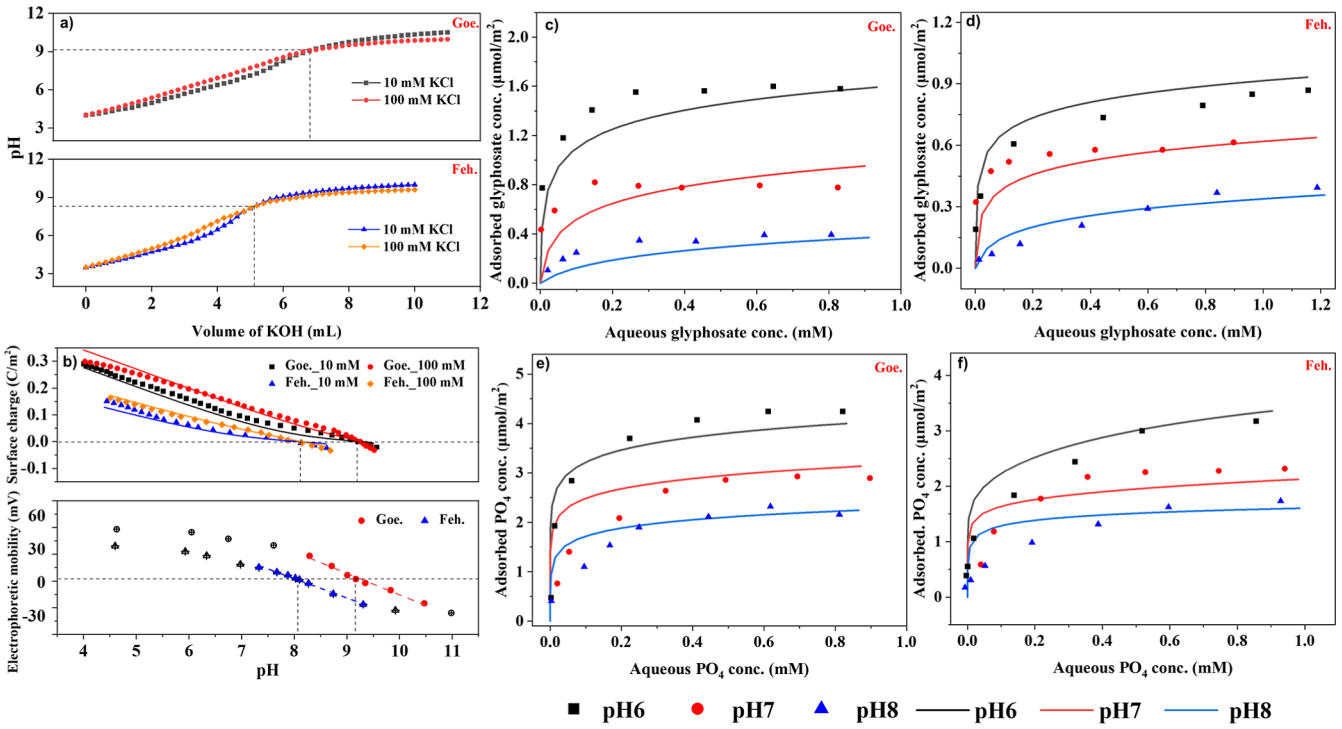


**Figure 1.** Surface characterization and model validation for goethite and ferrihydrite. (a) Acid−base titration curves at 10, 100 mM KCl; (b) charging behaviors (10, 100 mM KCl) and electrophoretic mobility (5 mM KCl). Adsorption isotherms of (c,d) Gly, and (e,f) $PO_4$ on goethite and ferrihydrite at pH 6, 7, and 8. Dots are experimental results and curves are simulated results.

balance in the presence of goethite. The isoelectric point ($pH_{IEP}$) of the minerals was determined using the Zetasizer Nano ZSP (Panalytical, Malvern, United Kingdom) by plotting zeta potential as a function of pH and regressing the linear portion of the data sets. The $pH_{IEP}$ was subsequent compared with point of zero charge ($pH_{pzc}$) derived from titration.

The CD-MUSIC model quantitatively analyzes ligand binding affinities at mineral/water interfaces, incorporating electrostatic effects within the Stern layer, as well as the capacitances of the inner and outer-layer, into its framework. The Stern layer is partitioned into two distinct regions, represented by planes 0, 1, and 2. Consideration of both singly and triply coordinated sites on the mineral surface is typically required for iron minerals. For the synthesized goethite, the surface sites were represented bysingly (≡FeOH) and triply (≡$Fe_3O$) coordinated surface groups, which reflect the predominant terminal and triple-bridge oxygen configurations on its predominant crystal faces, as established by crystallographic and spectroscopic studies. Its site densities ($N_s$) of 3.45 and 2.7 sites $nm^{-2}$, respectively, were applied in the CD-MUSIC model.[37] For ferrihydrite, site densities of 5.8 and 1.4 sites $nm^{-2}$ were used, following the CD-MUSIC model developed by Hiemstra and Zhao.[38] The ≡FeOH sites were further divided into two distinct types based on their capacity to form different surface complexes: edge-sharing sites (≡$FeO_eH$, $N_s$ = 3.0 sites $nm^{-2}$), which can form both mono- and bidentate complexs, and corner-sharing sites (≡$FeO_cH$, $N_s$ = 2.8 sites $nm^{-2}$), which can form only monodentate complexes. The parameters log K for $H^+$, $K^+$, and $Cl^-$, as well as the capacitance ($C_1$ for inner, $C_2$ for outer) values for the extended Stern layer model, were optimized using UCODE coupled to a modified version of FITEQL2.[39] The optimization followed a stepwise strategy: initial values were taken from the characterized mineral properties and published data for analogous systems; subsequently, only a constrained set of parameters were adjusted to achieve the best fit to the specific mineral charging behavior. The results are provided in Tables 1 and 2.

In modeling the Gly and $PO_4$ sorption, deprotonated monodentate (M), deprotonated bidentate (B), protonated monodentate (MH), protonated bidentate (BH), and doubly protonated monodentate ($MH_2$) complexes were considered for both iron hydroxides. Notably, bidentate complexes are assumed to form with ≡$FeO_cH$ on ferrihydrite.[38] In the modeling of $Fe^{2+}$ sorption, electron transfer from $Fe^{2+}$ to $Fe^{3+}$ was reported during the sorption process (B + $e^-$).[19] Additionally, tridentate (T) complexes can form via interaction with two ≡FeOH and one ≡$Fe_3O$ site (double edge sharing).[20] All considered surface complexation reactions and their corresponding


https://doi.org/10.1021/acsestwater.6c00065
ACS EST Water 2026, 6, 2018−2028

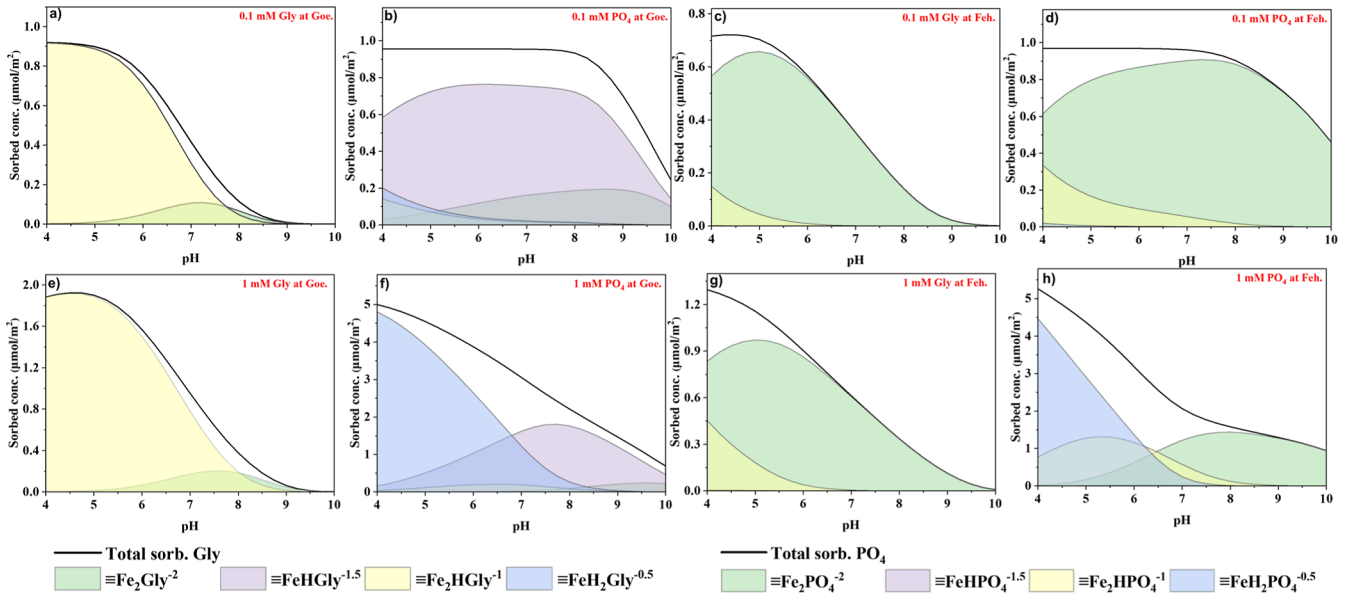


**Figure 2.** Simulated adsorption edge and surface complexation of Gly and $PO_4$ on goethite and ferrihydrite at initial conc. of (a–d) 0.1 mM and (e–h) 1 mM.

log K for Gly, $PO_4$, and $Fe^{2+}$ were optimized using Visual Minteq 3.1 coupled with PEST.[40,41] Atmospheric $CO_2$ level of 410 ppm was incorporated into all CD-MUSIC simulations to account for its influence on aqueous carbonate speciation and proton balance under experimentally relevant conditions. The charge distribution to the surface, inner Stern plane, and outer Stern plane ($\Delta z_0$, $\Delta z_1$, $\Delta z_2$) are sourced from the papers reported by Hiemstra and co-workers and are summarized in Tables 1 and 2. The aqueous speciation and possible surface complexation structures of Gly and $PO_4$ are illustrated in Figure S5, Table S1 and Figure S6.

## 3. RESULTS AND DISCUSSION

### 3.1. Comparative Analysis of CD-MUSIC Parameters

In previous studies, the CD-MUSIC model has been applied to goethite and ferrihydrite, taking into account factors such as SSA, $pH_{pzc}$, $N_s$, and C. Table 3 compares CD-MUSIC parameters from the literature with the final optimized set obtained in this study. For our systems, the SSA, $pH_{pzc}$ values were fixed inputs, while the parameters $N_s$ and C are the results of optimizing the model against our acid–base titration data. For goethite, our synthesized material exhibited a significantly lower SSA compared to earlier reports (42 $m^2/g$ vs–90 $m^2/g$) by Geysels & Hiemstra[28] and Rahnemaie & Hiemstra,[42] which directly led to comparatively lower overall adsorption in our experiments. Nonetheless, our study helps fill the knowledge gap regarding goethite with moderate SSA, providing a useful reference for understanding the environmental behavior of goethite across different particle sizes. This finding is consistent with observations by Wang et al.[43] for microsized goethite (23 $m^2/g$), which also exhibited differences in C values compared to high-SSA goethite—a trend echoed in our modeled C1 value being higher than those from studies using ~90 $m^2/g$ goethite. For ferrihydrite, our fitted CD-MUSIC parameters show good consistency with those reported by Hiemstra & Zhao[38] and by Gustafsson & Antelo.[32] For our modeling, the SSA of ferrihydrite was set to 611 $m^2/g$, representing the typical surface area of fresh, nonfreeze–dried ferrihydrite rather than the BET-measured value of the freeze–dried sample (275.2 $m^2/g$), to accurately reflect the material state in our adsorption experiments. It is worth noting, however, that Antelo et al.[44] investigated aged ferrihydrite and applied BET-SSA, which may account for some differences in model parameters. Although our ferrihydrite parameters are comparable to literature values, this study aims to apply CD-MUSIC model to Gly adsorption on ferrihydrite—both individually and in competition with $PO_4$ and $Fe^{2+}$—thereby providing novel mechanistic insight into Gly retention under complex conditions.

### 3.2. Mineral Surface Charge Behavior and Single Solute Sorption

Figure 1 illustrates the surface properties and adsorption behavior of goethite and ferrihydrite through integrated experimental and modeling approaches. The potentiometric titration curves in 10 and 100 mM KCl (Figure 1a) intersect at 9.25 for goethite and 8.01 for ferrihydrite, providing an estimate of the $pH_{pzc}$.[45] Crucially, these $pH_{pzc}$ values are in excellent agreement with the $pH_{IEP}$ independently determined from the pH-dependence of electrophoretic mobility (Figure 1b). This consistency between two distinct experimental methods supports the assignment of the $pH_{pzc}$. While the CD-MUSIC model optimization yields discernible log K values for $K^+$ and $Cl^-$ (Tables 1 and 2), the convergence of the titration intersection and the $pH_{IEP}$ indicates that, at the macroscopic level, the net effect of electrolyte ion adsorption on the proton-conditional surface charge is minimal around the $pH_{pzc}$ for our systems. The surface charging behaviors in Figure 1b) were described by the CD-MUSIC model, revealing distinct electrical layer structures: goethite exhibits higher inner capacitance ($C_1$ = 1.65 $C/m^2$) but lower outer capacitance ($C_2$ = 0.74 $C/m^2$) compared to ferrihydrite ($C_1$ = 1.15 $C/m^2$, $C_2$ = 0.90 $C/m^2$). The fundamental difference in their $pH_{pzc}$ reflects the contrasting surface protonation behavior between the crystalline goethite and amorphous ferrihydrite structures. The $pH_{pzc}$-derived log K for $H^+$ were subsequently used in the adsorption modeling. A broader comparison of $pH_{pzc}$ with literature values is provided in Table S2.


https://doi.org/10.1021/acsestwater.6c00065
ACS EST Water 2026, 6, 2018–2028

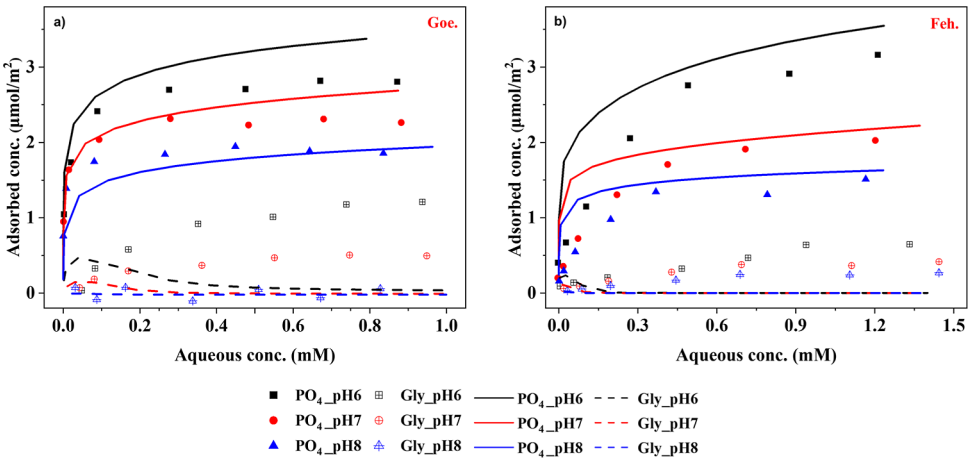


**Figure 3.** Competitive binary sorption from equimolar Gly-$PO_4$ mixtures on (a) goethite and (b) ferrihydrite at pH 6, 7, and 8. Dots are experimental results and curves are simulated results.

Figure 1c–f presents multiple adsorption isotherms for Gly and $PO_4$ determined at different pH values,[6−8] demonstrating decreasing adsorption with increasing pH[6−8] at iron hydroxides. This behavior primarily results from the decrease in positive surface charge as pH approaches the $pH_{pzc}$, leading to weakened electrostatic interactions between the mineral surfaces and anionic adsorbates. $PO_4$ exhibits higher uptake compared to Gly onto minerals, consistent with previous reports on soils.[46,47] The close match between experimental data points and CD-MUSIC model simulations (solid curves) confirms model reliability in predicting surface complexation behavior under varying chemical conditions (evaluated by $R^2$, Table S4). It is noted that the model shows slight deviations from experimental data at low concentrations. These discrepancies may be related to the enhanced influence of intrinsic surface site heterogeneity at low coverage, which is challenging to fully capture with an averaged site density model. Nevertheless, across the full range of conditions studied, the CD-MUSIC model provides a quantitatively superior description of the adsorption data compared to alternative diffuse layer model (DLM) formulations (see comparative analysis in the Supporting Information). This comprehensive data set provides critical parameters for understanding contaminant adsorption mechanisms in iron hydroxide-dominated environmental systems. Additionally, surface complexation corresponding to adsorption isotherms was simulated in Figures S7 and S8. Surface sites occupied during adsorption, as calculated from experimental data, were compared with $N_s$ implemented in the CD-MUSIC model (Table S3).

### 3.3. Surface Complexation of Single Gly, $PO_4$

Modeling parameters listed in Tables 1 and 2 can be used to calculate the speciation of Gly and $PO_4$ complexes on goethite and ferrihydrite surfaces as a function of pH and initial concentration. Figure 2a–h explore adsorption behaviors at representative initial concentrations of 0.1 mM (low loading) and 1 mM (high loading).

Our model reveals that, across the entire pH range and at the studied concentrations (0.1−1 mM), Gly predominantly presents on the goethite surface in BH and B forms, with the contribution of the B complex becoming increasingly prominent as pH increases (Figure 2a,e). This trend is mechanistically driven by the deprotonation of the—$NH_2$ group, which is the sole structural difference between the B and BH configurations (See Figure S6). These findings are consistent with the most recent results reported by Geysels and Hiemstra for Gly adsorption on goethite,[28] who also considered a comprehensive set of surface species including B, BH, MH, and $MH_2$. In our study, the contributions of MH and $MH_2$ complexes were optimized to be negligible, whereas they constituted a minor proportion in the cited work.[28] The inclusion of $MH_2$ in our goethite model followed the same comprehensive approach to ensure a complete description of protonation equilibria. This discrepancy in minor species distribution is not due to the CD values—which were sourced from Rahnemaie et al.[42] but is rationally explained by distinct physicochemical properties of the goethite samples. Specifically, our material has a lower SSA (41.9 $m^2/g$ vs 94 $m^2/g$) and a different $C_1$ (1.65 $F/m^2$ vs 0.83 $F/m^2$) (Table 3). Similarly, Gly is mainly complexed on ferrihydrite in BH and B forms, with B complex being the dominant species (Figure 2c,g). Earlier research[48] using ATR-FTIR and XANES for adsorption speciation analysis yielded results consistent with ours, indicating that at low pH, binding occurs preferentially via the B complex, while at common pH, both B and MH complexes are predominant. Notably, on both iron minerals, the Gly surface species do not exhibit strong concentration dependence.

In contrast, MH and $MH_2$ complexes contribute significantly to $PO_4$ adsorption. As shown in Figure 2b, the MH complex dominates $PO_4$ adsorption at low loading conditions, while the $MH_2$ complex is the secondary contributor under acidic pH. The proportion of B rises with increasing pH, becoming comparable to the MH complex at pH 10. Numerous DFT studies[17,42,49,50] have investigated $PO_4$ adsorption on goethite, all of which concluded that M bonding is the optimal geometry for $PO_4$. However, a critical limitation of DFT lies in its reliance on finite molecular computations, which hinders accurate prediction of high-concentration adsorption behavior. Our analysis reveals a notable shift at high loading (Figure 2f), where $MH_2$ replaces MH as the dominant complex in acidic pH. This transition is mechanistically attributed to reduced electrostatic potential in the Stern layer under elevated surface loading, which enhances proton adsorption and facilitates $MH_2$ complex formation. Intriguingly, $PO_4$ adsorption on ferrihydrite at low loading is predominantly mediated by B and BH complexes. (Figure 2d), which is consistent with the results


https://doi.org/10.1021/acsestwater.6c00065
ACS EST Water 2026, 6, 2018−2028

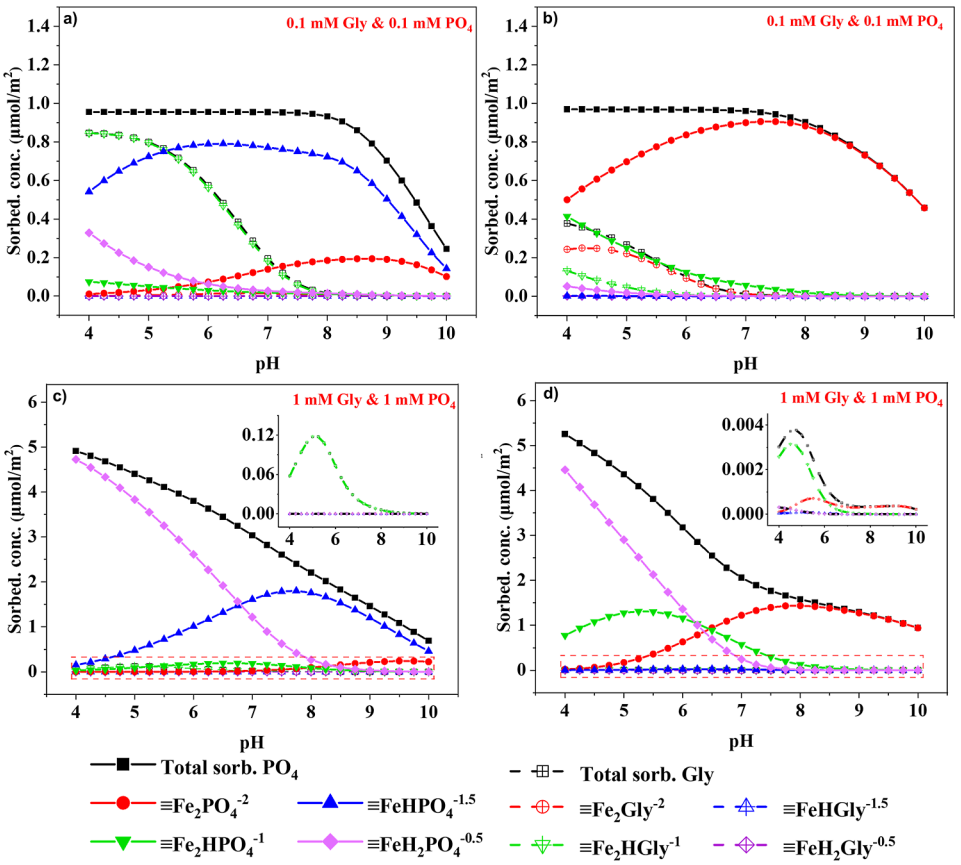


**Figure 4.** Simulated adsorption edge and surface complexation of Gly vs $PO_4$ on goethite and ferrihydrite at initial conc. of (c,e) 0.1 mM and (d,f) 1 mM. Dots are experimental results and curves are simulated results.

previously reported by Antelo et al.[44] Discrepancies emerge at high pH, where their model suggests minor M-type contributions—a divergence traceable to differences in material properties between studies: $pH_{pzc}$ (8.0 vs 8.1), SSA (611 $m^2/g$ vs 229 $m^2/g$), and $C_1$ (1.15 $F/m^2$ vs 0.74 $F/m^2$). At high loading, the contribution of the $MH_2$ complex to $PO_4$ adsorption on ferrihydrite under acidic conditions becomes non-negligible, as illustrated in Figure 2h). Additionally, CD-MUSIC model predictions indicate that $PO_4$ adsorption remains less pH-independent under low-concentration acidic conditions, and both Gly and $PO_4$ exhibit generally decreasing adsorption trends across the pH 4−10 range in other scenarios, consistent with typical anion adsorption behavior on iron minerals.

Based on CD-MUSIC model simulation results, it is clear that the adsorption and complexation of Gly and $PO_4$ on iron hydroxides are jointly influenced by environmental pH, mineral type, and initial concentration in the system.

### 3.4. Binary Sorption and Complexation of Gly and $PO_4$

To analyze competitive adsorption between Gly and $PO_4$ on the two iron minerals, we simultaneously added equal concentrations of both adsorbates to mineral suspensions at different pH.[6−8] The results are shown in Figure 3a,b, where dots represent experimental data and curves denote CD-MUSIC model simulations. In the competitive adsorption system, both Gly and $PO_4$ exhibited decreasing adsorption with rising pH, while $PO_4$ consistently demonstrated stronger affinity than Gly across all pH conditions. Interestingly, the model accurately predicted $PO_4$ adsorption trends but showed discrepancies in Gly adsorption behavior. Experimentally, despite the presence of strongly adsorbing $PO_4$, Gly partially remained adsorbed on iron minerals, where the CD-MUSIC model predicted full Gly desorption under competitive conditions. This persistent uptake under strong competition is consistent with the irreversible adsorption behavior observed for Gly on other mineral surfaces such as $\gamma$-$Al_2O_3$,[51] where dedicated desorption and mass balance experiments confirmed a nonlabile fraction. We also considered the possibility of Gly decomposition contributing to the apparent retention; however, this is unlikely under our experimental conditions (pH 6−8, 12 h) as our analytical method (IC-ECD) did not detect significant levels of its primary abiotic degradation product (AMPA), and such conditions are not known to promote rapid degradation. Therefore, the observed discrepancy suggests that some Gly-mineral complexes exhibit irreversible binding characteristics not captured by the equilibrium CD-MUSIC model.

The surface speciation in Figure 4a−d provides insight into the model underestimation of Gly adsorption in binary systems. In 0.1 mM competitive systems, (Figure 4a,c) Gly maintained measurable adsorption competition against $PO_4$. Although Gly adsorption decreased, Gly surface species remained consistent with single-adsorbate systems across pH conditions. (Figure 2a,c) At higher concentrations (1 mM, Figure 4b,d), $PO_4$ maintained its single system behavior and surface species, (Figure 2f,h) while Gly adsorption dropped sharply with peak adsorption occurring near pH 5. The model predicted a shift in dominant Gly surface species to BH-type complexes under these conditions (Figure 4b,d) and


https://doi.org/10.1021/acsestwater.6c00065
ACS EST Water 2026, 6, 2018−2028

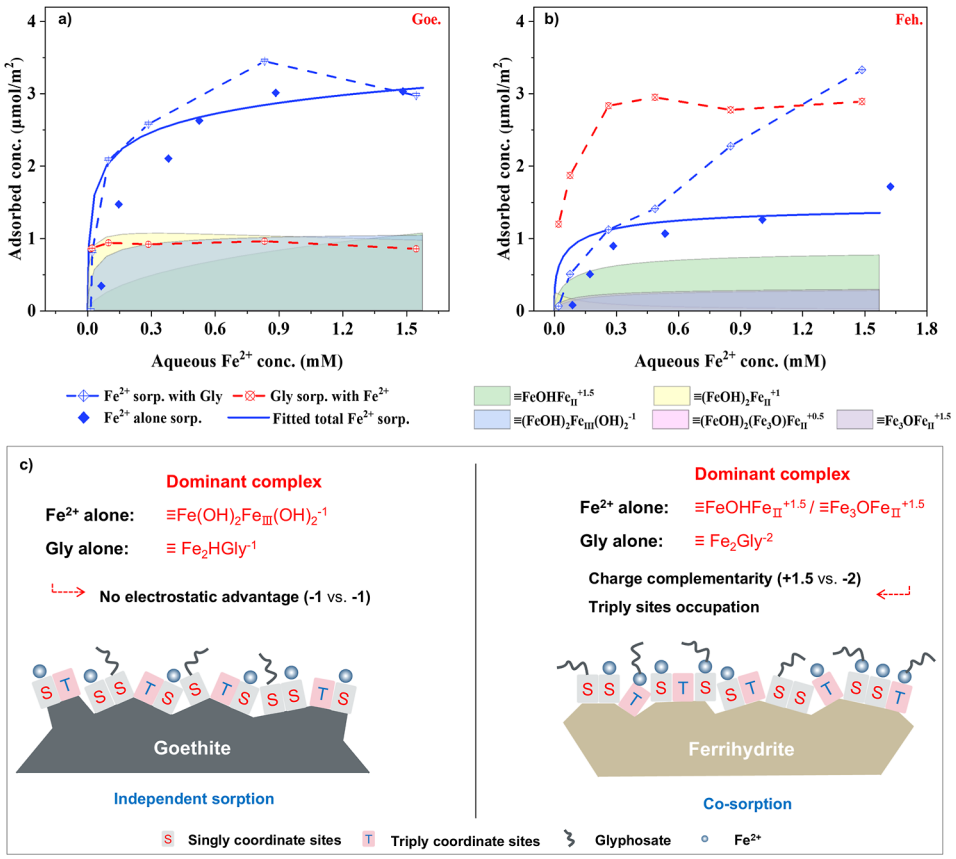


**Figure 5.** Simulated $Fe^{2+}$ adsorption isotherm and surface complexation on (a) goethite and (b) ferrihydrite under isothermal conditions at pH 7. Solid lines represent $Fe^{2+}$ single adsorption, while dashed lines indicate $Fe^{2+}$ adsorption in competition with pre-equilibrated Gly (0.24 mM). Stacked bars depict the relative contributions of $Fe^{2+}$ surface species at pH 7 along the single adsorption isotherm. (c) Schematic illustration of the proposed binary sorption mechanism for $Fe^{2+}$ and Gly at iron minerals.

potentially reflected irreversible complexation at high concentrations.

Until now, no existing models have fully predicted the Gly-$PO_4$ competitive adsorption patterns observed here. Previous CD-MUSIC studies have primarily focused on individual Gly[28] or $PO_4$[26,43,44] adsorption on iron minerals, as well as selected inorganic binary systems such as $Mg^{2+}/Ca^{2+}$-$PO_4$,[52] As(V)-$PO_4$,[32] whereas the Gly-$PO_4$ organic–inorganic competition remained less modeled. Recent work[53] is beginning to address this complexity by developing a CD-MUSIC framework for Gly adsorption on ferrihydrite in the presence of $PO_4$, and under a Gly concentration of 0.47 mM, a noticeable decline in model performance is found. Moreover, a complementary study[54] from the same group demonstrated that glyphosate adsorption on metal (hydr)oxide surfaces is subject to pronounced steric hindrance effects, which become increasingly important at higher surface coverages. Such steric constraints can limit access to reactive surface sites and alter surface complexation configurations, mechanisms that are not explicitly accounted for in conventional CD-MUSIC formulations. Together, these findings highlight the inherent challenges of modeling large, multifunctional organic adsorbates in competitive systems and help explain why the equilibrium CD-MUSIC model employed in this study underestimates the irreversible fraction of Gly binding. This limitation likely arises from the omission of steric effects and molecular crowding phenomena in addition to classical site competition and electrostatic interactions. By extending CD-MUSIC to this unexplored domain, our work provides new experimental and modeling insights for organic–inorganic competitive adsorption systems.

### 3.5. Binary Sorption and Surface Complexation of $Fe^{2+}$

$Fe^{2+}$ is widely present in natural environments, especially abundant under anoxic and reducing conditions, while it readily oxidizes to $Fe^{3+}$ in oxygenated waters.[9] $Fe^{2+}$ primarily exists in soil–water systems of wetlands, paddy fields, and sediments under reducing conditions, playing a crucial role in biogeochemical cycling.[55−57] $Fe^{2+}$-sorbed on iron hydroxides can significantly enhance the transformation of organic pollutants and stabilize organic carbon through adsorption and coprecipitation mechanisms. Previous studies have shown that $Fe^{2+}$ barely reacts with ligands ($Cl^-$, $OH^-$) in natural waters at ambient pH.[58] Given that $Fe^{2+}$ forms complexes with Gly in solution,[10] (Figure S9) with no reports of solid $Fe^{2+}$-Gly precipitation under analogous conditions, this study investigates the competitive adsorption behavior between $Fe^{2+}$ and Gly under the premise of preadsorption of Gly.

The dissolution of minerals during adsorption was also analyzed in Figure S10, indicating that it was negligible and all measured $Fe^{2+}$ concentrations originated from experimental additions. In Figure 5, the adsorption of $Fe^{2+}$ on iron minerals alone and under Gly competitive conditions is presented, with the complexation of $Fe^{2+}$ illustrated as stacked diagrams. On goethite (Figure 5a), $Fe^{2+}$ adsorption was not affected by the presence of preadsorbed Gly, resulting in a similar overall uptake as when $Fe^{2+}$ was adsorbed alone. At pH 7, Gly


https://doi.org/10.1021/acsestwater.6c00065
ACS EST Water 2026, 6, 2018−2028

primarily forms the BH complex carrying a −1 charge, while $Fe^{2+}$ mainly coordinates via a B form with two $\equiv FeOH^{-0.5}$ sites (−1 charge) on the goethite surface (Figure 5c). This leads to no electrostatic advantage via Gly preadsorption to influence $Fe^{2+}$ binding. In contrast, on ferrihydrite (Figure 5b), the adsorption amounts of both $Fe^{2+}$ and Gly increased under coadsorption conditions compared to their single system adsorption. This indicates that $Fe^{2+}$ and Gly mutually enhance their adsorption on ferrihydrite. In this case, Gly predominantly forms the B complex with a −2 charge, while $Fe^{2+}$ mainly binds in the M form (+1.5 charge) on ferrihydrite (Figure 5c). This enhanced opposite charge complementarity between the adsorbed species facilitates coadsorption. Furthermore, when optimizing $Fe^{2+}$ adsorption on ferrihydrite using the CD-MUSIC model, we also considered its complexation with $\equiv Fe_3O^{-0.5}$. Without including this interaction, the predicted adsorption amounts were significantly lower than the experimental data. Therefore, these sites are also potential coadsorption sites for $Fe^{2+}$ and Gly on ferrihydrite.

Previous studies have reported that other divalent metal ions, such as $Ca^{2+}$,[59,60] $Cd^{2+}$,[61] $Mg^{2+}$,[60] $Zn^{2+}$,[62] etc., influence $PO_4$ adsorption on both goethite and ferrihydrite. According to our charge results for the simulated surface species, one explanation can be that $PO_4$ forms the MH complex with goethite at pH 7 carrying a −1.5 charge, giving those cations an electrostatic advantage over $Fe^{2+}$ for surface binding (−0.5 charge). The same mechanism can be applied to explain coadsorption behavior on ferrihydrite. As pointed out, the effects of $Fe^{2+}$ on Gly adsorption on iron hydroxides remain rarely studied. Most existing research has focused on how $Cu^{2+}$,[63] $Zn^{2+}$,[64] $Pb^{2+}$[65] influence Gly adsorption in soils, often showing that these cations enhance the environmental mobility of Gly under most conditions. Therefore, the dual mineral-specific roles exhibited by $Fe^{2+}$ in its adsorption and complexation behaviors, as demonstrated by the application of the CD-MUSIC model in this study, provide new insights and theoretical foundations for understanding $Fe^{2+}$ transport in the environment.

## 4. ENVIRONMENTAL IMPLICATIONS

To address the competitive effects of $PO_4$ and $Fe^{2+}$ on Gly adsorption and the associated modeling challenges, we applied the CD-MUSIC framework to experimental data for goethite and ferrihydrite. Our results demonstrate that $PO_4$ exhibits stronger affinity than Gly for both iron hydroxides, with their surface bonding governed by pH, initial concentration, mineral type, and competitive interactions. This implies that $PO_4$ fertilization in agroecosystems can thus limit the retention of Gly in iron-rich soils, while natural $PO_4$ cycling in aquatic and terrestrial systems may critically regulate Gly mobility. The incomplete desorption of Gly under strong $PO_4$ competition highlights its environmental persistence; the proposed complexation mechanism provides new insights into its long-term fate.

Co-adsorption experiments with $Fe^{2+}$ revealed dual roles: $Fe^{2+}$ enhances Gly adsorption on ferrihydrite but has negligible effects on goethite. As iron hydroxides are key components controlling nutrient and contaminant retention and transport in soils, and $Fe^{2+}$ is predominantly enriched in anoxic environments such as wetlands and rice paddies, our findings deepen the understanding of Gly mobility under reducing conditions. This study also extends the application of the CD-MUSIC model to organic−inorganic competitive systems. While the model successfully describes the dominant trends and identifies key surface species, it underestimates Gly retention under strong competition. This discrepancy highlights the current limitation of equilibrium-based models in fully capturing mechanisms such as steric hindrance or specific irreversible binding, which may operate at high surface coverage. Overall, the optimized parameters and mechanistic insights provided here constitute a critical advance for modeling Gly fate in complex, iron-rich environments and enhance the predictive capability of SCMs for multicomponent systems.

## ■ ASSOCIATED CONTENT

### Supporting Information

The Supporting Information is available free of charge at https://pubs.acs.org/doi/10.1021/acsestwater.6c00065.

Details about the characterization of iron hydroxides, speciation and surface complexation of absorbates, dissolution of minerals during adsorption, comparison of CD-MUSIC parameters, and fitting comparison between DLM and CD-MUSIC model (PDF)

## ■ AUTHOR INFORMATION


### Corresponding Author

**Stefan B. Haderlein** − *Geo- and Environmental Research Center, Department of Geosciences, Eberhard Karls Universität Tübingen, Tübingen 72076, Germany;* orcid.org/0000-0002-9309-8523; Email: stefan.haderlein@uni-tuebingen.de

### Authors

**Mingshuai Wang** − *Geo- and Environmental Research Center, Department of Geosciences, Eberhard Karls Universität Tübingen, Tübingen 72076, Germany;* orcid.org/0000-0002-9919-4348

**Johannes Lützenkirchen** − *Institute for Nuclear Waste Disposal, Karlsruhe Institute of Technology, Eggenstein-Leopoldshafen 76344, Germany;* orcid.org/0000-0002-0611-2746

Complete contact information is available at: https://pubs.acs.org/10.1021/acsestwater.6c00065


### Notes

The authors declare no competing financial interest.

## ■ ACKNOWLEDGMENTS

We thank Tsz Ho Chiu for performing BET and XRD measurements, and Anna Röhnelt for her assistance with MP-AES. Further, we are grateful to Dr. Philipp Martin and Dr. Daniel Buchner for their careful discussions during the experimental work. We also acknowledge the broader surface complexation modeling community for their foundational contributions. This research was supported by the China Scholarship Council (CSC).

## ■ REFERENCES

(1) Antier, C.; Andersson, R.; Auskalniene, O.; Barić, K.; Simić, M. A survey on the uses of glyphosate in European countries. *ENDURE network* **2020**, 1−60.

(2) Aparicio, V. C.; De Geronimo, E.; Marino, D.; Primost, J.; Carriquiriborde, P.; Costa, J. L. Environmental fate of glyphosate and

aminomethylphosphonic acid in surface waters and soil of agricultural basins. *Chemosphere* **2013**, *93* (9), 1866−1873.
(3) Feltracco, M.; Barbaro, E.; Morabito, E.; Zangrando, R.; Piazza, R.; Barbante, C.; Gambaro, A. Assessing glyphosate in water, marine particulate matter, and sediments in the Lagoon of Venice. *Environ. Sci. Pollut. Res. Int.* **2022**, *29* (11), 16383−16391.
(4) Mac Loughlin, T. M.; Peluso, M. L.; Aparicio, V. C.; Marino, D. J. G. Contribution of soluble and particulate-matter fractions to the total glyphosate and AMPA load in water bodies associated with horticulture. *Sci. Total Environ.* **2020**, *703*, 134717.
(5) Zhang, Q.; Li, Y.; Kroeze, C.; Xu, W.; Gai, L.; Vitsas, M.; Ma, L.; Zhang, F.; Strokal, M. A global assessment of glyphosate and AMPA inputs into rivers: Over half of the pollutants are from corn and soybean production. *Water Res.* **2024**, *261*, 121986.
(6) Gimsing, A. L.; Borggaard, O. K. Competitive adsorption and desorption of glyphosate and phosphate on clay silicates and oxides. *Clay Minerals* **2002**, *37* (3), 509−515.
(7) Wimmer, B.; Neidhardt, H.; Schwientek, M.; Haderlein, S. B.; Huhn, C. Phosphate addition enhances alkaline extraction of glyphosate from highly sorptive soils and aquatic sediments. *Pest Manage. Sci.* **2022**, *78* (6), 2550−2559.
(8) Hua, J.; Sun, J.; Chen, M. J.; Liu, C. S.; Wu, F. Aqueous Fe(II)-catalyzed iron oxide recrystallization: Fe redox cycling and atom exchange, mineralogical recrystallization and contributing factor. *Rev. Environ. Sci. Bio/Technol.* **2023**, *22* (1), 55−78.
(9) Gorski, C. A.; Scherer, M. M. Fe2+ sorption at the Fe oxide-water interface: A revised conceptual framework. In *Aquatic Redox Chemistry*; ACS Publications, 2011; pp 315−343.
(10) Popov, K.; Rönkkömäki, H.; Lajunen, L. H. J. Critical evaluation of stability constants of phosphonic acids (IUPAC technical report). *Pure Appl. Chem.* **2001**, *73* (10), 1641−1677.
(11) Sheals, J.; Sjoberg, S.; Persson, P. Adsorption of glyphosate on goethite: molecular characterization of surface complexes. *Environ. Sci. Technol.* **2002**, *36* (14), 3090−3095.
(12) Barja, B. C.; Dos Santos Afonso, M. Aminomethylphosphonic acid and glyphosate adsorption onto goethite: a comparative study. *Environ. Sci. Technol.* **2005**, *39* (2), 585−592.
(13) Yan, W.; Jing, C. Molecular Insights into Glyphosate Adsorption to Goethite Gained from ATR-FTIR, Two-Dimensional Correlation Spectroscopy, and DFT Study. *Environ. Sci. Technol.* **2018**, *52* (4), 1946−1953.
(14) Ahmed, A. A.; Leinweber, P.; Kuhn, O. Unravelling the nature of glyphosate binding to goethite surfaces by ab initio molecular dynamics simulations. *Phys. Chem. Chem. Phys.* **2018**, *20* (3), 1531−1539.
(15) Kwon, K. D.; Kubicki, J. D. Molecular orbital theory study on surface complex structures of phosphates to iron hydroxides: calculation of vibrational frequencies and adsorption energies. *Langmuir* **2004**, *20* (21), 9249−9254.
(16) Kubicki, J. D.; Kwon, K. D.; Paul, K. W.; Sparks, D. L. Surface complex structures modelled with quantum chemical calculations: carbonate, phosphate, sulphate, arsenate and arsenite. *Eur. J. Soil Sci.* **2007**, *58* (4), 932−944.
(17) Ahmed, A. A.; Gypser, S.; Freese, D.; Leinweber, P.; Kuhn, O. Molecular level picture of the interplay between pH and phosphate binding at the goethite-water interface. *Phys. Chem. Chem. Phys.* **2020**, *22* (45), 26509−26524.
(18) Ahmed, A. A.; Morshedizad, M.; Kuhn, O.; Leinweber, P. Deciphering competitive interactions: Phosphate and organic matter binding on goethite through experimental and theoretical insights. *Sci. Total Environ.* **2024**, *940*, 173510.
(19) Hiemstra, T.; van Riemsdijk, W. H. Adsorption and surface oxidation of Fe(II) on metal (hydr)oxides. *Geochim. Cosmochim. Acta* **2007**, *71* (24), 5913−5933.
(20) Dixit, S.; Hering, J. G. Sorption of Fe(II) and As(III) on goethite in single- and dual-sorbate systems. *Chem. Geol.* **2006**, *228* (1−3), 6−15.
(21) Hiemstra, T.; VanRiemsdijk, W. H. A surface structural approach to ion adsorption: The charge distribution (CD) model. *J. Colloid Interface Sci.* **1996**, *179* (2), 488−508.
(22) Goli, E.; Rahnemaie, R.; Hiemstra, T.; Malakouti, M. J. The interaction of boron with goethite: experiments and CD-MUSIC modeling. *Chemosphere* **2011**, *82* (10), 1475−1481.
(23) Mendez, J. C.; Hiemstra, T. High and low affinity sites of ferrihydrite for metal ion adsorption: Data and modeling of the alkaline-earth ions Be, Mg, Ca, Sr, Ba, and Ra. *Geochim. Cosmochim. Acta* **2020**, *286*, 289−305.
(24) Zhao, W.; Tan, W.; Wang, M.; Xiong, J.; Liu, F.; Weng, L.; Koopal, L. K. CD-MUSIC-EDL Modeling of Pb(2+) Adsorption on Birnessites: Role of Vacant and Edge Sites. *Environ. Sci. Technol.* **2018**, *52* (18), 10522−10531.
(25) Hiemstra, T.; Barnett, M. O.; van Riemsdijk, W. H. Interaction of silicic acid with goethite. *J. Colloid Interface Sci.* **2007**, *310* (1), 8−17.
(26) Jin, J.; Xiong, J.; Liang, Y.; Wang, M.; Huang, C.; Koopal, L.; Tan, W. Generic phosphate affinity constants of the CD-MUSIC-eSGC model to predict phosphate adsorption and dominant speciation on iron (hydr)oxides. *Water Res.* **2024**, *264*, 122194.
(27) Lian, W.; Yu, G.; Ma, J.; Xiong, J.; Niu, C.; Zhang, R.; Xie, H.; Weng, L. Quantitative Insights into Phosphate-Enhanced Lead Immobilization on Goethite. *Environ. Sci. Technol.* **2024**, *58* (26), 11748−11759.
(28) Geysels, B.; Hiemstra, T.; Groenenberg, J. E.; Comans, R. N. J. Glyphosate binding and speciation at the water-goethite interface: A surface complexation model consistent with IR spectroscopy and MO/DFT. *Water Res.* **2025**, *273*, 123031.
(29) Schwertmann, U.; Cornell, R. *Iron Oxides in the Laboratory*; VCH: Weinheim Germany, 1991.
(30) Raven, K. P.; Jain, A.; Loeppert, R. H. Arsenite and arsenate adsorption on ferrihydrite: Kinetics, equilibrium, and adsorption envelopes. *Environ. Sci. Technol.* **1998**, *32* (3), 344−349.
(31) Strehlau, J. H.; Toner, B. M.; Arnold, W. A.; Penn, R. L. Accessible reactive surface area and abiotic redox reactivity of iron oxyhydroxides in acidic brines. *Geochim. Cosmochim. Acta* **2017**, *197*, 345−355.
(32) Gustafsson, J. P.; Antelo, J. Competitive Arsenate and Phosphate Adsorption on Ferrihydrite as Described by the CD-MUSIC Model. *ACS Earth Space Chem.* **2022**, *6* (5), 1397−1406.
(33) Murphy, J.; Riley, J. P. A modified single solution method for the determination of phosphate in natural waters. *Anal. Chim. Acta* **1962**, *27*, 31−36.
(34) Porsch, K.; Kappler, A. FeII oxidation by molecular $O_2$ during HCl extraction. *Environ. Chem.* **2011**, *8* (2), 190−197.
(35) Stookey, L. L. Ferrozine-a new spectrophotometric reagent for iron. *Anal. Chem.* **1970**, *26*, 1534−1538.
(36) Lützenkirchen, J.; Preočanin, T.; Kovačević, D.; Tomišić, V.; Lövgren, L.; Kallay, N. Potentiometric Titrations as a Tool for Surface Charge Determination. *Croat. Chem. Acta* **2012**, *85* (4), 391−417.
(37) Hiemstra, T.; Antelo, J.; Rahnemaie, R.; Riemsdijk, W. H. v. Nanoparticles in natural systems I: The effective reactive surface area of the natural oxide fraction in field samples. *Geochim. Cosmochim. Acta* **2010**, *74* (1), 41−58.
(38) Hiemstra, T.; Zhao, W. Reactivity of ferrihydrite and ferritin in relation to surface structure, size, and nanoparticle formation studied for phosphate and arsenate. *Environ. Sci.:Nano* **2016**, *3* (6), 1265−1279.
(39) Poeter, E. E.; Hill, M. C.; Banta, E. R.; Mehl, S.; Christensen, S. *UCODE_2005 and Six Other Computer Codes for Universal Sensitivity Analysis, Calibration, and Uncertainty Evaluation Constructed Using the JUPITER API*; US Geological Survey, 2005.
(40) Gustafsson, J. P. *Visual MINTEQ 3.0 User Guide*; KTH, Department of Land and Water Recources: Stockholm, Sweden, 2011; Vol. *550*.
(41) Doherty, J. E. *Model-Independent Parameter Estimation User Manual Part II: PEST Utility Support Software*; Watermark: Brisbane, Australia, 2016; Vol. *268*.


https://doi.org/10.1021/acsestwater.6c00065
*ACS EST Water* 2026, 6, 2018−2028

(42) Rahnemaie, R.; Hiemstra, T.; van Riemsdijk, W. H. Geometry, charge distribution, and surface speciation of phosphate on goethite. *Langmuir* **2007**, *23* (7), 3680−3689.
(43) Wang, F.; Xu, J.; Xu, Y.; Chen, H.; Liang, Y.; Xiong, J. Face-dependent phosphate speciation on goethite: CD-MUSIC modeling and ATR-FTIR/2D-COS study. *Sci. Total Environ.* **2024**, *915*, 169970.
(44) Antelo, J.; Fiol, S.; Perez, C.; Marino, S.; Arce, F.; Gondar, D.; Lopez, R. Analysis of phosphate adsorption onto ferrihydrite using the CD-MUSIC model. *J. Colloid Interface Sci.* **2010**, *347* (1), 112−119.
(45) Bourikas, K.; Vakros, J.; Kordulis, C.; Lycourghiotis, A. Potentiometric mass titrations: Experimental and theoretical establishment of a new technique for determining the point of zero charge (PZC) of metal (hydr)oxides. *J. Phys. Chem. B* **2003**, *107* (35), 9441−9451.
(46) Gimsing, A. L.; Borggaard, O. K.; Bang, M. Influence of soil composition on adsorption of glyphosate and phosphate by contrasting Danish surface soils. *Eur. J. Soil Sci.* **2004**, *55* (1), 183−191.
(47) Munira, S.; Farenhorst, A.; Akinremi, W. Phosphate and glyphosate sorption in soils following long-term phosphate applications. *Geoderma* **2018**, *313*, 146−153.
(48) Li, X.; Yang, P.; Zhao, W.; Guo, F.; Jaisi, D. P.; Mi, S.; Ma, H.; Lin, B.; Feng, X.; Tan, W.; et al. Adsorption Mechanisms of Glyphosate on Ferrihydrite: Effects of Al Substitution and Aggregation State. *Environ. Sci. Technol.* **2023**, *57* (38), 14384−14395.
(49) Chen, P.; Song, D.; Zhang, X.; Xie, Q.; Zhou, Y.; Liu, H.; Xu, L.; Chen, T.; Rosso, K. M. Understanding Competitive Phosphate and Silicate Adsorption on Goethite by Connecting Batch Experiments with Density Functional Theory Calculations. *Environ. Sci. Technol.* **2022**, *56* (2), 823−834.
(50) Kubicki, J. D.; Paul, K. W.; Kabalan, L.; Zhu, Q.; Mrozik, M. K.; Aryanpour, M.; Pierre-Louis, A. M.; Strongin, D. R. ATR-FTIR and density functional theory study of the structures, energetics, and vibrational spectra of phosphate adsorbed onto goethite. *Langmuir* **2012**, *28* (41), 14573−14587.
(51) Wang, M.; Wang, L.; Martin, P. R.; Buchner, D.; Lützenkirchen, J.; Meixner, A. J.; Haderlein, S. B. Mechanisms and reversibility of glyphosate and phosphorus ligands sorption on Al2O3: Experimental evidence and computational modeling. *Water Res.* **2026**, *289*, 124799.
(52) Atouei, M. T.; Rahnemaie, R.; Kalanpa, E. G.; Davoodi, M. H. Competitive adsorption of magnesium and calcium with phosphate at the goethite water interface: Kinetics, equilibrium and CD-MUSIC modeling. *Chem. Geol.* **2016**, *437*, 19−29.
(53) Geysels, B.; Hiemstra, T.; Vermeer, A. W.; Groenenberg, J. E. A mechanistic surface complexation model for glyphosate adsorption to ferrihydrite in competition with phosphate. *Water Res.* **2026**, *288*, 124634.
(54) Geysels, B.; Groenenberg, J. E.; Hiemstra, T.; Apreza Arrieta, H. S.; Vermeer, A. W.; Comans, R. N. Steric hindrance of glyphosate adsorption to metal (hydr) oxides: A novel model approach for organic matter-mineral interactions. *Environ. Sci. Technol.* **2025**, *59* (27), 14020−14029.
(55) Clement, J.; Shrestha, J.; Ehrenfeld, J.; Jaffe, P. Ammonium oxidation coupled to dissimilatory reduction of iron under anaerobic conditions in wetland soils. *Soil Biol. Biochem.* **2005**, *37* (12), 2323−2328.
(56) Shuai, W.; Jaffe, P. R. Anaerobic ammonium oxidation coupled to iron reduction in constructed wetland mesocosms. *Sci. Total Environ.* **2019**, *648*, 984−992.
(57) Zhou, G. W.; Yang, X. R.; Li, H.; Marshall, C. W.; Zheng, B. X.; Yan, Y.; Su, J. Q.; Zhu, Y. G. Electron Shuttles Enhance Anaerobic Ammonium Oxidation Coupled to Iron(III) Reduction. *Environ. Sci. Technol.* **2016**, *50* (17), 9298−9307.
(58) Millero, F. J.; Yao, W. S.; Aicher, J. The Speciation of Fe(Ii) and Fe(Iii) in Natural-Waters. *Mar. Chem.* **1995**, *50* (1−4), 21−39.
(59) Rietra, R. P.; Hiemstra, T.; van Riemsdijk, W. H. Interaction between calcium and phosphate adsorption on goethite. *Environ. Sci. Technol.* **2001**, *35* (16), 3369−3374.
(60) Mendez, J. C.; Hiemstra, T. Ternary Complex Formation of Phosphate with Ca and Mg Ions Binding to Ferrihydrite: Experiments and Mechanisms. *ACS Earth Space Chem.* **2020**, *4* (4), 545−557.
(61) Venema, P.; Hiemstra, T.; van Riemsdijk, W. H. Interaction of Cadmium with Phosphate on Goethite. *J. Colloid Interface Sci.* **1997**, *192* (1), 94−103.
(62) Van Eynde, E.; Hiemstra, T.; Comans, R. N. J. Interaction of Zn with ferrihydrite and its cooperative binding in the presence of PO4. *Geochim. Cosmochim. Acta* **2022**, *320*, 223−237.
(63) Dousset, S.; Jacobson, A. R.; Dessogne, J. B.; Guichard, N.; Baveye, P. C.; Andreux, F. Facilitated transport of diuron and glyphosate in high copper vineyard soils. *Environ. Sci. Technol.* **2007**, *41* (23), 8056−8061.
(64) Wang, Y. J.; Zhou, D. M.; Sun, R. J.; Cang, L.; Hao, X. Z. Cosorption of zinc and glyphosate on two soils with different characteristics. *J. Hazard Mater.* **2006**, *137* (1), 76−82.
(65) Si, Y. B.; Xiang, Y.; Tian, C.; Si, X. Y.; Zhou, J.; Zhou, D. M. Complex Interaction and Adsorption of Glyphosate and Lead in Soil. *Soil Sediment Contam* **2013**, *22* (1), 72−84.




https://doi.org/10.1021/acsestwater.6c00065
*ACS EST Water* 2026, 6, 2018−2028